

# I

## A new phase of matter?

### 1 Micro-bang and big-bang

#### 1.1 Energy and time scales

When atomic nuclei, generally called heavy-ions, collide at very high energies, such that the kinetic energy exceeds significantly the rest energy, dense hadronic\* matter is produced. We refer to these reactions as (ultra)relativistic heavy-ion, or nuclear, collisions. The energy density of hadronic matter with which we are concerned has a benchmark value of

$$\epsilon = 1 \text{ GeV fm}^{-3} = 1.8 \times 10^{15} \text{ g cm}^{-3}. \quad (1.1)$$

The corresponding relativistic matter pressure is

$$P \simeq \frac{1}{3}\epsilon = 0.52 \times 10^{30} \text{ bar}. \quad (1.2)$$

Dense matter with these properties must have existed in the early Universe about 10  $\mu\text{s}$  after the big-bang. It might have been recreated extremely rarely in interactions of very-high-energy cosmic-ray particles. Some astrophysical objects may reach these extreme conditions. It had been speculated that a catastrophic change in the Universe could ensue when these conditions are recreated in laboratory experiments, but these fears have been refuted [85].

Experimental study of the physics of the early Universe requires in principle a large, practically infinite, volume of matter. For this reason, it is necessary to study high-energy collisions of the heaviest nuclei, rather than the more elementary and simpler-to-handle interactions of protons or leptons. However, we cannot study in the laboratory physical systems

---

\* In Greek, *barys* means strong and heavy; *leptos* is weak, light; *mesos* is intermediate, and *hadros* is strong. Hadronic (strong) interactions involve baryons and mesons (heavy and semi-heavy particles) but not leptons, the light and relatively weakly interacting electrons, muons, the heavy tau, and nearly massless neutrinos.

larger in volume than lead (Pb) or gold (Au). Hence, it would seem that we will not be able to explore experimentally the properties of the phase transition involving the dissolution of hadronic particles, since it is known that genuine phase transitions cannot develop in finite physical systems. However, only for *non-relativistic finite systems* it is impossible to observe experimentally the discontinuous phase properties. In our case, the ability to produce particles from energy and the presence of virtual fluctuation effects greatly enhance the number of physical states accessible. We therefore hope to identify in collisions of relativistic heavy-ions a (nearly) singular manifestation of a phase transition from the nuclear, hadronic phase to a matter phase consisting of quarks and gluons.

We use units in which the Boltzmann constant  $k = 1$ . In consequence, the temperature  $T$  is discussed in units of energy, which, in this book, are either MeV  $\simeq 2m_e c^2$  ( $m_e$  is the electron mass) or GeV = 1000 MeV  $\simeq m_N c^2$  ( $m_N$  is the mass of a nucleon). The conversion scale of typical temperature involves ten additional zeros:

$$100 \text{ MeV} \equiv 116 \times 10^{10} \text{ K}. \quad (1.3)$$

To appreciate the magnitude of this temperature, let us recall that the center of the Sun is believed to be at  $T = 11 \times 10^6 \text{ K}$ , and the scale of temperature of interest to us is in fact 100 000 times greater.

In general, the units in this book are chosen such that the numerical values  $\hbar = c = 1$ , e.g., the mass of particles will also be measured in units of energy and the energy density can appear as the fourth power of an energy unit. With the conversion factor  $\hbar c = 0.197 \text{ GeV fm}$ , the reference energy density in normal nuclei is

$$\frac{m_N}{V_N} = 0.17 m_N \text{ fm}^{-3} \simeq 0.16 \text{ GeV fm}^{-3} = 1.27 \times 10^{-4} \text{ GeV}^4. \quad (1.4)$$

Experimental results have shown that ultra-relativistic heavy-ion collisions lead to the formation of a dense hadronic fireball, well localized in space, with an energy density exceeding  $1 \text{ GeV fm}^{-3}$ . Such a spatially localized drop of highly excited, hot, and dense *elementary matter* will be rapidly evolving, indeed exploding, driven by the high internal pressure. The fireball has a short life span characterized by the size of the system  $\tau \simeq 2R/c$ .

In relativistic heavy-ion reactions, the collision energy is shared among numerous newly produced hadronic particles. Therefore, in the final state we observe many soft (low-energy) newly produced hadronic particles, rather than a few particles of high-energy as is the case in hard, elementary interactions. An important objective of our research is the understanding of the processes that lead to the conversion of kinetic collision energy into high particle multiplicity. Because of the large numbers of

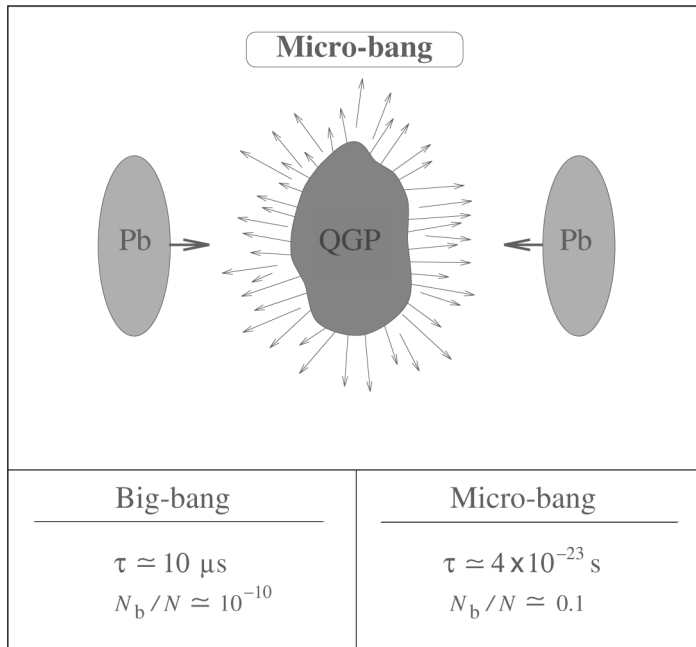


Fig. 1.1. Top: Lorentz-contracted nuclei collide in the center-of-momentum frame and form a region of dense matter, which evolves into a final state of hadrons. Bottom: two key differences involving baryon number  $N_b$  and total particle number  $N$  between the micro-bang and the cosmological big-bang.

particles produced, many thousands in recent experiments, we believe that this can be accomplished using statistical mechanics. This method has the advantage that it does not require a complete description of the microscopic production and dynamics of particles. It will be introduced in great detail in this book.

A qualitative image of the high-energy nuclear-collision ‘micro-bang’ is depicted in Fig. 1.1: two nuclei are shown, Lorentz-contracted in the direction of motion, approaching from two sides and colliding in the center-of-momentum (CM) laboratory frame, forming a region of dense matter (dark-shaded), the fireball. Subsequently, the collective expansion flow of fireball matter develops, and evolves in the final state into free streams of individual particles, indicated by individual arrows.

The temporal evolution of a fireball into a final state comprising a multitude of different hadronic particles is similar to, though much faster than, the corresponding stage in the evolution of the early Universe. Relativistic heavy-ion collision leads to a rapidly evolving fireball of quark–gluon plasma (QGP), in which the short time scale involved is probed by the equilibration of abundance of quark flavors. We can not hope to be able

to recreate the ‘slow big-bang’ of the Universe in the laboratory in the last detail. Our objective is to obtain precise information about the physical processes and parameters which govern the rapidly changing hadronic phase. Within a theoretical framework, we can hope to unravel what happened when the Universe hadronized.

The bottom portion of Fig. 1.1 reminds us of the two important differences between the two ‘bangs’, the big-bang of the Universe and the micro-bangs generated in the nuclear-collision experiments.

1. The time scale of the expansion of the Universe is determined by the interplay of the gravitational forces and the radiative and Fermi pressure of the hot matter, whereas in the micro-bangs there is no gravitation to slow the expansion, which lasts at most about  $10^{-22}$  s. The time scale of the heavy-ion collision, indicated in Fig. 1.1, suggests that the size and the (local) properties of the exploding nuclear fireball must change rapidly even on the scale of hadronic interactions, contrary to the situation in the early Universe. It is convenient to represent the expansion time constant  $\tau_U$  of the Universe in terms of the Newtonian gravitational constant  $G$  and the vacuum energy  $\mathcal{B}$ :

$$\tau_U = \sqrt{\frac{3c^2}{32\pi G\mathcal{B}}} = 36\sqrt{\frac{\mathcal{B}_0}{\mathcal{B}}} \mu\text{s}, \quad \mathcal{B}_0 = 0.19 \text{ GeV fm}^{-3} = (195 \text{ MeV})^4. \quad (1.5)$$

The range of values of the ‘bag’ constant  $\mathcal{B}$  found in the literature,  $145 \text{ MeV} < \mathcal{B}^{1/4} < 235 \text{ MeV}$ , leads to  $66 \mu\text{s} > \tau_U > 25 \mu\text{s}$ .

2. The early radiative Universe was practically baryonless, whereas in the laboratory we create a fireball of dense matter with a considerable baryon number  $N_b$  per total final particle multiplicity  $N$ . Thus, unlike in the early Universe, we expect in a laboratory micro-bang a significant matter–antimatter asymmetry in particle abundance. The matter–antimatter symmetry of particle spectra is in turn an important indicator suggesting that the matter–antimatter symmetry has been restored in other aspects.

The matter–antimatter-abundance asymmetry is easily overcome theoretically, since it implies a relatively minor extrapolation of the baryochemical potential  $\mu_b$  introduced to fix the baryon density. In fact, RHIC experiments at CM-energy 130A GeV per pair of nucleons ( $\sqrt{s_{NN}} = 130 \text{ GeV}$ ) are already much more baryon–antibaryon symmetric than the SPS condition where  $\sqrt{s_{NN}} \leq 17.3 \text{ GeV}$ , and the highest RHIC and LHC energies will allow us to extrapolate our understanding from  $\mu_b/T \leq 1$  to  $\mu_b/T \ll 1$ .

More difficult to resolve will be the differences in the physics due to the different time scales involved. The evolution of the Universe is slow on

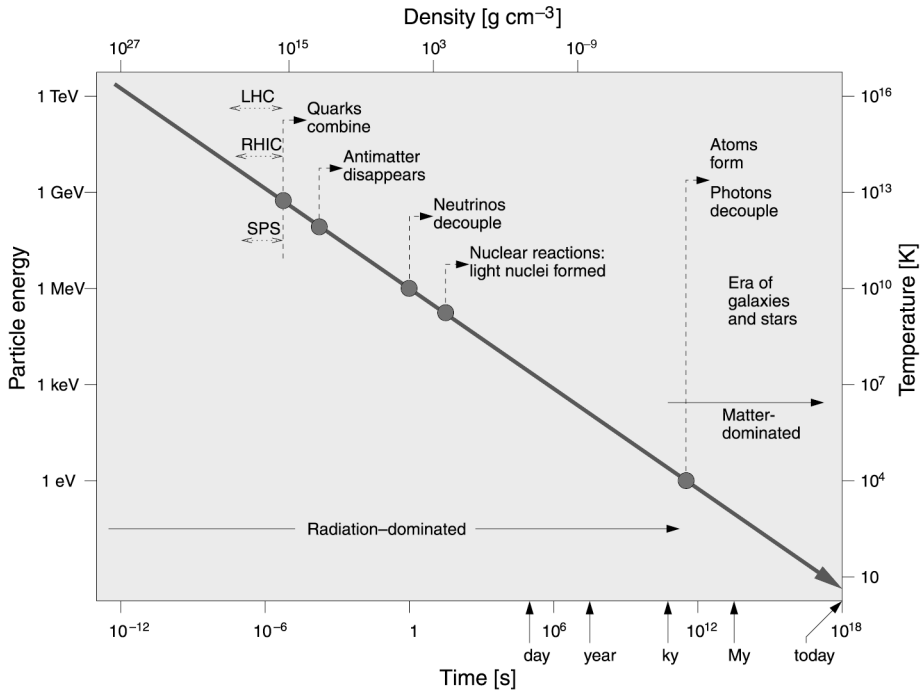


Fig. 1.2. Particle energy (temperature) as a function of time in the early Universe. Different evolutionary epochs are shown along with the accessible range of accelerator laboratory experiments.

the hadronic time scale. Given the value of  $\tau_U$ , we expect that practically all unstable hadronic particles decay, all hadronic equilibria are fully attained, and there is potentially time to develop macroscopic structures in the ‘mixed phase’ of QGP and hadronic gas (HG), and for weak interactions to take place. All this can not occur during the life span of the dense matter created in nuclear collisions.

The temporal evolution of the Universe is depicted, in Fig. 1.2, as a function of time. Beginning with decoupling of neutrinos and nucleosynthesis at time  $\mathcal{O}(1)$ s the evolution of the Universe is well understood today. In comparison, little work has gone into the detailed understanding of the earlier period when the nearly symmetric matter–antimatter hadron gas emerged from the quark–gluon phase and evolved into the baryon Universe in which we find ourselves today. This period spans the temperature interval  $300 \text{ MeV} < T < 1 \text{ MeV}$ , separating the perturbative QGP epoch from the epoch of decoupling of neutrinos and cosmological nucleosynthesis.

We see, in Fig. 1.2, that, after about  $10 \mu\text{s}$ , the deconfined phase of quarks and gluons is transformed into a hot gas of hadrons, namely mesons,

baryons, and antibaryons. Just after that, the evolution of our Universe was marked by a period of baryon–antibaryon annihilation, and, possibly, separation: although we have not been able to observe antimatter in our galaxy, or in the neighborhood of our galaxy, it is far from certain that there is no antimatter in our Universe.

The laboratory study of the formation of the QGP and hadronization is expected to lead to an understanding of how the hot, baryon- and antibaryon-rich hadron gas evolved after its formation at  $T \simeq 170$  MeV. Employing the statistical-physics methods developed in this book, one finds that the energy fraction of baryons and antibaryons within hadronic-gas matter is about 25% just after the QGP has hadronized in the early Universe, and nearly half of this is comprised of the heavier and unstable strange baryons and antibaryons. It is believed that this strong antimatter component disappears from the Universe prior to the era of nucleosynthesis.

## 1.2 Quarks and gluons

Both quarks and gluons manifest themselves only for a short instant following a high-energy interaction, and have never been observed as free objects at macroscopic distances from the space–time volume of the reaction; they are ‘confined’. Gluons interact only through strong interactions and pose a great experimental challenge regarding the study of their properties. The measurement of the properties of confined quarks is relatively easy, since, in addition to the strong-interaction (color) charge, they also carry the electro-weak charges.

There are six different *flavors* of quarks, see table 1.1, two practically stable flavors referred to as *up* – for the proton-like quark  $u$ , and *down* – for the neutron-like quark  $d$ . We often refer to these two light quarks by their generic name  $q$ . Light quarks  $q$  may be viewed as a single entity with two states, up or down. The semi-heavy *strange*-flavor  $s$ -quark decays due to electro-weak interaction when it is bound in hadrons, typically within  $10^{-10}$  s, whereas the heavier *charm*  $c$  and *bottom*  $b$  flavors have approximate life spans of  $3 \times 10^{-13}$  s and  $10^{-12}$  s, respectively.

These six flavors of quarks form three doublets:

$$\begin{pmatrix} u \\ d \end{pmatrix}, \quad \begin{pmatrix} c \\ s \end{pmatrix}, \quad \begin{pmatrix} t \\ b \end{pmatrix}; \quad Q_q = \begin{pmatrix} +\frac{2}{3} \\ -\frac{1}{3} \end{pmatrix}.$$

The upper component of a doublet has charge  $Q_q = +\frac{2}{3}$ , in units of the proton charge, whereas the lower component has one unit of charge less, as is also the case for the related lepton doublet comprising the three charged leptons (electron, muon, and tau) accompanied by their neutrinos. There is an antiquark for each quark, carrying the opposite electrical charge.

Table 1.1. Properties of quarks: flavor  $f$  symbol, flavor name, electrical charge  $Q_f$  (in units of proton charge  $Q_p$ ), and mass  $m_f$  at energy scale 2 GeV; see the text for further discussion of strange-quark mass

$f$	Quark	$Q_f [Q_p]$	$m_f(2 \text{ GeV})$
u	Up	$+\frac{2}{3}$	$3.5 \pm 2 \text{ MeV}$
d	Down	$-\frac{1}{3}$	$6 \pm 3 \text{ MeV}$
s	Strange	$-\frac{1}{3}$	$115 \pm 55 \text{ MeV}$
c	Charm	$+\frac{2}{3}$	$1.25 \pm 0.15 \text{ GeV}$
b	Bottom	$-\frac{1}{3}$	$4.25 \pm 0.15 \text{ GeV}$
t	Top	$+\frac{2}{3}$	$174.3 \pm 5.1 \text{ GeV}$

Quarks differ from charged leptons (electrons  $e$ , muons  $\mu$ , and taus  $\tau$ ), and neutrinos ( $\nu_i$ ,  $i = e, \mu$ , and  $\tau$ ) by a further internal quantum number they must carry, in addition to spin. The presence of this additional quantum number arises even in the simplest quark models. For example, consider hadronic particles containing three quarks of the same flavor, such as the spin-3/2 baryons:

$$\Delta^{++} = (uuu), \quad \Delta^- = (ddd), \quad \Omega^- = (sss).$$

The physical properties of these baryons imply that three identical quarks are present in the same S-wave with the same spin wave function. Since quarks are fermions, they are subject to the Pauli principle. Thus, there must be an additional way to distinguish the quarks, aside from spin. This additional degeneracy factor has been determined to be  $g_c = 3$ . It became known as the color of quarks – in analogy to the three fundamental colors: red, green, and blue.

Color is an internal quantum number, which like the electrical charge, is thought to be the source of a force [123]. It seems that there is no way to build an apparatus to distinguish the three fundamental color charges, all colors must everywhere be exactly equal physically. The theory of color forces must satisfy the principle of local nonabelian gauge invariance, e.g., invariance under arbitrary local  $SU(3)$  transformations in the three-dimensional color space. In other aspects, there is considerable formal similarity with quantum electrodynamics (QED). Therefore, the theory of strong interactions based on such color forces has been called quantum chromodynamics (QCD).

The flavor structure and symmetry of quarks and leptons remains a mystery today. We also do not have a fundamental understanding of the origin of quark masses. In table 1.1 we see that quarks of various flavors

differ widely in their ‘current’ mass  $m_f$ , that is mass which enters the elementary QCD Lagrangian  $\mathcal{L}_{\text{QCD}}$ . The values presented in table 1.1 are for the momentum scale 2 GeV.

Since quarks are confined inside hadrons, and the zero-point energy of confinement is much larger than the masses of light quarks, their masses could not be determined by direct measurement. However, the precise masses of light u and d quarks do not matter in the study of hadronic interactions, being generally much smaller than the pertinent energy scales,

The mass of the strange quark  $m_s$  is barely heavy enough to be determined directly in a study of hadronic structure. We adopt, in this book, the value  $m_s(1 \text{ GeV}) = 200 \pm 20 \text{ MeV}$  [150]. In the value of  $m_s$  reference is made to the scale of energy at which the mass of the strange quark is measured: akin to the interaction strength, also the mass of quarks depends on the (energy) scale. This value of  $m_s$  corresponds to  $m_s(2 \text{ GeV}) \simeq m_s(1 \text{ GeV})/1.30 = 154 \pm 15 \text{ MeV}$ . A somewhat smaller value  $m_s(2 \text{ GeV}) = 115 \pm 55 \text{ MeV}$ , see table 1.1, corresponding to  $m_s(1 \text{ GeV}) \simeq 150 \pm 70 \text{ MeV}$ , is the recommended value. The rather rapid change by 30% of the quark mass between the 1- and 2-GeV scales is well known, but often not remembered, e.g., the ‘low’ recommended mass of the charmed quark presented in table 1.1 in fact corresponds to  $m_c(1 \text{ GeV}) = 1.6 \text{ GeV}$ , a rather ‘high’ value.

### 1.3 The hadronic phase transition in the early Universe

We will now show that the ‘freezing’ of quark–gluon ‘color’ deconfined degrees of freedom is the essential ingredient in determining the conditions in a transition between phases that has time to develop into equilibrium. The following discussion tacitly assumes the presence of latent heat  $\mathcal{B}$  in the transition, and a discontinuity in the number of degrees of freedom,  $g_2 \neq g_1$ , where ‘1’ refers to the primeval QGP phase and ‘2’ to the final hadronic-gas state.

To find the phase-transition point, we determine the (critical) temperature at which the pressures in the two phases are equal. We allow, in a transition of first order, for a difference in energy density  $\epsilon_1 \neq \epsilon_2$  associated with the appearance of latent heat  $\mathcal{B}$  (the ‘bag constant’), which also enters the pressure of the deconfined phase. We consider the Stefan–Boltzmann pressure of a massless photon-like gas with degeneracy  $g_i$ :

$$P_c \equiv P_1(T_c) = \frac{\pi^2}{90} g_1 T_c^4 - \mathcal{B}, \quad (1.6)$$

$$P_c \equiv P_2(T_c) = \frac{\pi^2}{90} g_2 T_c^4. \quad (1.7)$$

We obtain

$$\frac{\mathcal{B}}{T_c^4} = \frac{\pi^2}{90} \Delta g, \quad T_c = \mathcal{B}^{\frac{1}{4}} \left( \frac{90}{\pi^2 \Delta g} \right)^{\frac{1}{4}}, \quad \Delta g = g_1 - g_2. \quad (1.8)$$

The transition temperature, in the early Universe, is slightly higher than the value seen in laboratory experiments, even though Eq. (1.8) involves only the difference in the number of degrees of freedom. For the pressure at the transition we obtain

$$P_c = \mathcal{B} \frac{g_2}{\Delta g}. \quad (1.9)$$

The pressure, and therefore the dynamics of the transition in the early Universe, depends on the presence of non-hadronic degrees of freedom, which are absent from laboratory experiments with heavy ions.

In summary, the phase-transition dynamics in the early Universe is determined by

- (a) the effective number of confined degrees of freedom,  $g_2$ , at  $T_c$ ;
- (b) the change in the number of acting degrees of freedom  $\Delta g$ , which occurs exclusively in the strong-interaction sector; and
- (c) the vacuum pressure (latent heat)  $\mathcal{B}$ , a property of strong interactions.

In order to understand the early Universe, we need to measure these quantities in laboratory experiments.

Both phases involved in the hadronization transition contain effectively massless electro-weak (EW) particles. Even though the critical temperature does not depend on the background of EW particles not participating in the transition, the value of the critical pressure, Eq. (1.9), depends on this, and thus we will briefly digress to consider the active electro-weak degrees of freedom. These involve photons,  $\gamma$ , and all light fermions, viz.,  $e$ ,  $\mu$ ,  $\nu_e$ ,  $\nu_\mu$ , and  $\nu_\tau$  (we exclude the heavy  $\tau$ -lepton with  $m_\tau \gg T$ , and we consider the muon as being effectively a massless particle). Near to  $T \simeq 200$  MeV, we obtain

$$g^{\text{EW}} = g_\gamma + \frac{7}{4} g_{\text{F}}^{\text{EW}} = 14.25, \quad (1.10)$$

with

$$g_\gamma = 2, \quad \frac{7}{4} g_{\text{F}}^{\text{EW}} = \frac{7}{8} \times 2 \times (2_e + 2_\mu + 3_\nu) = 12.25,$$

where charged, effectively massless fermions enter with spin multiplicity 2, and we have three neutrino flavors – there are only left-handed light neutrinos and right-handed antineutrinos, and thus only half as many neutrino degrees of freedom as would naively be expected.

In the deconfined QGP phase of the early Universe, we have

$$g_1 = g^{\text{EW}} + g_g + \frac{7}{4} g_{\text{q}}. \quad (1.11)$$

The number of effectively present strongly interacting degrees of freedom of quarks and gluons is influenced by their interactions, characterized by the strong coupling constant  $\alpha_s$ , and this book will address this topic in depth,

$$g_g = 2_s \times 8_c \left(1 - \frac{15}{4\pi} \alpha_s\right), \quad \frac{7}{4} g_q = \frac{7}{4} 2_s \times 2.5_f \times 3_c \left(1 - \frac{50}{21\pi} \alpha_s\right), \quad (1.12)$$

where the flavor degeneracy factor used is 2.5, allowing in a qualitative manner for the contribution of more massive strangeness; table 1.1. The degeneracies of quarks and gluons are indicated by the subscripts s(pin) and, c(olor), respectively. We obtain

$$g_1 = \begin{cases} 56.5, & \text{for } \alpha_s = 0, \\ \sim 37, & \text{for } \alpha_s = 0.5, \\ \sim 33, & \text{for } \alpha_s = 0.6. \end{cases} \quad (1.13)$$

For the QCD perturbative interactions with  $\alpha_s = 0.5\text{--}0.6$ , we see that  $g_1 \simeq 35 \pm 2$ .

We now consider the final HG phase of the early Universe: there is no light, strongly interacting fermion. Aside from three light bosons (pions  $\pi^\pm$  and  $\pi^0$ ), the presence of heavier hadrons contributes at  $T \lesssim 170$  MeV, and one finds for the hadronic degrees of freedom  $g_2^h \simeq 5$

$$g_2 \equiv g^{\text{EW}} + g_2^h \simeq 19. \quad (1.14)$$

Thus, we find from Eqs. (1.13) and (1.14),

$$g_1 - g_2 = \Delta g = \begin{cases} \sim 37, & \text{for } \alpha_s = 0, \\ \sim 18, & \text{for } \alpha_s = 0.5, \\ \sim 14, & \text{for } \alpha_s = 0.6. \end{cases} \quad (1.15)$$

For the QCD perturbative interactions with  $\alpha_s = 0.5\text{--}0.6$ , we see that about half of the degrees of freedom freeze across the transition in the early Universe.

For the value  $\mathcal{B}^{1/4} = 190$  MeV and  $\alpha_s \simeq 0.5$ , we obtain from Eq. (1.8) a transition temperature  $T_c \simeq 160$  MeV. At this temperature, the critical pressure Eq. (1.9) is found to be  $P_c \simeq 1.4 \mathcal{B}$ , and it includes both hadronic and electro-weak partial pressure contributions. The hadronic fractional pressure present in laboratory experiments and seen in lattice simulations of gauge theories (compare with section 15.5) is  $P_c^h \simeq \mathcal{B}/4$ .

### 1.4 Entropy-conserving (isentropic) expansion

Much of the time dependence of an expanding Universe is related to the assumption of adiabatic, i.e., entropy-conserving, expansion dynamics:

$$dE + P dV = T dS = 0, \quad dE = d(\epsilon V), \quad \frac{dV}{V} = \frac{3 dR}{R}. \quad (1.16)$$

Here, as usual,  $\epsilon$  is the energy density in the local restframe, and the three-dimensional volume element  $dV$  scales with the third power of the distance scale  $R$ . We obtain

$$\frac{3 dR}{R} = -\frac{d\epsilon}{\epsilon + P}. \quad (1.17)$$

We will revisit Eq. (1.17) which describes general expansion dynamics of the micro-bang.

We now relate the expansion dynamics to the velocity of sound, and use well known relations of thermodynamics which we will discuss in this book,

$$d\epsilon = \frac{d\epsilon}{dP} \frac{dP}{dT} dT = \frac{1}{v_s^2} \sigma dT = \frac{1}{v_s^2} \frac{\epsilon + P}{T} dT. \quad (1.18)$$

We will revisit the derivation Eq. (1.18) when we study the same physics occurring in the expansion of the dense-matter phase formed in heavy-ion collisions in section 6.3. Using Eq. (1.17), we obtain

$$\frac{3 dR}{R} = -\frac{1}{v_s^2} \frac{dT}{T}. \quad (1.19)$$

This equation allows the integral

$$RT^{1/(3v_s^2)} = \text{constant}, \quad (1.20)$$

which describes exactly how the temperature decreases in an isentropic expansion once the equation of state  $P = P(\epsilon)$ , and hence the velocity of sound is known.

For a relativistic equation of state,  $v_s^2 = \frac{1}{3}$  and thus

$$R(t)T(t) = \text{constant}, \quad V(t)T^3(t) = \text{constant}. \quad (1.21)$$

While this result applies to a three-dimensional expansion, it is easily generalized to a one-dimensional expansion, such as is expected to apply in ultra-high-energy heavy-ion collisions.

## 1.5 The dynamic Universe

The  $(\mathbf{0}, \mathbf{0})$ -component of the Einstein equation,

$$\mathcal{R}_{\mu\nu} - \frac{1}{2}g_{\mu\nu}\mathcal{R} + \Lambda_{\nu}g_{\mu\nu} = 8\pi GT_{\mu\nu}, \quad (1.22)$$

gives the Friedmann equation which determines the rate of expansion of the homogeneous Universe,

$$H^2(t) \equiv \left(\frac{\dot{R}}{R}\right)^2 = \frac{8\pi G}{3}\epsilon + \frac{\Lambda_{\nu}}{3} - \frac{k}{R^2}. \quad (1.23)$$

In the last term,  $k = 0, 1$ , and  $-1$  for different geometries of the Universe (flat, bubble, and hyperbolic-open); this term is negligible in our considerations.  $\Lambda_v$  is Einstein’s cosmological term, which is playing a similar dynamic role to  $\mathcal{B}$ , but, in comparison, it is of irrelevant magnitude during the early time period we consider.  $H$  is the Hubble ‘constant’ which varies with time. Its present-day value,  $H(t_0) = H_0$ , is of considerable interest and is given in the range

$$H_0 = 70 \pm 15 \text{ km s}^{-1} \text{ Mpc}^{-1} = \frac{0.7 \pm 0.15}{10^{10} \text{ y}} = (2.2 \pm 0.5) \times 10^{-17} \text{ s}^{-1}.$$

Inserting Eq. (1.17), with  $V \propto R^3$ , into Eq. (1.23) and neglecting the last two terms in Eq. (1.23), we find for  $\epsilon(t)$

$$\dot{\epsilon}^2 = 24\pi G\epsilon(\epsilon + P(\epsilon))^2. \tag{1.24}$$

We equate the particle energy density and pressure, including the vacuum term  $\mathcal{B}$  in the relativistic equation of state for the particle component,

$$\epsilon - \mathcal{B} \simeq \frac{\pi^2}{30}gT^4 \simeq 3(P + \mathcal{B}), \quad \epsilon = 3P + 4\mathcal{B}. \tag{1.25}$$

Thus,

$$\dot{\epsilon}^2 = \frac{128\pi G}{3} \epsilon(\epsilon - \mathcal{B})^2, \tag{1.26}$$

which is valid (approximately) both for QGP and for HG phases, but in the HG phase  $\mathcal{B} = 0$ .

Despite its highly nonlinear nature, Eq. (1.26) has an analytical solution,

$$\epsilon_1 = \mathcal{B} \coth^2(t/\tau_U), \tag{1.27}$$

where  $\tau_U$  is the expansion time constant we have defined in Eq. (1.5) and the subscript ‘1’ reminds us that Eq. (1.5) describes the evolution in the quark–gluon phase with  $\mathcal{B} \neq 0$ . At  $t < \tau_U$ , the energy density rises like  $1/t^2$ ; for  $t > \tau_U$ , it would remain constant at the vacuum energy density.

Once the transition to HG phase ‘2’ with  $\mathcal{B} \rightarrow \Lambda_v \sim 0$  has occurred, the analytical form of the solution changes; we exploit the singularity  $\coth x \rightarrow 1/x$  and obtain the power-law solution

$$\epsilon_2 = \mathcal{B} \left( \frac{\tau_U}{t} \right)^2 = \frac{3}{32\pi G} \frac{1}{t^2} = \frac{\pi^2}{30}g_2T^4. \tag{1.28}$$

In the middle of Eq. (1.28), we have substituted  $\tau_U$  from Eq. (1.5) to show that, in principle,  $\mathcal{B}$  does not enter the solution. On the right-hand side of Eq. (1.28), we show the energy density of the (radiation-dominated; see Fig. 1.2) Universe, establishing the well-known relation

$$\boxed{\left(\frac{t_2}{t}\right)^2 = \left(\frac{T}{T_c}\right)^4, \quad T \propto \frac{1}{\sqrt{t}}.} \tag{1.29}$$

Using Eq.(1.8) for  $T_c$ , we determine  $t_2$ , the time when the Universe entered the hadronic phase, which we use below in Eq.(1.33). Similarly we also obtain the behavior of the size of the Universe with time. By inserting Eqs.(1.27) and (1.28) into Eq.(1.23), we find how the scale  $R$  of the Universe evolves:

$$R^2 \propto \sinh\left(\frac{t}{\tau_U}\right) \Big|_1 \rightarrow \left(\frac{t}{\tau_U}\right) \Big|_2. \tag{1.30}$$

To determine when the transition between the two phases occurs, and how long it takes, we consider the pressure in both phases. In deconfined phase ‘1’ where  $\mathcal{B} \neq 0$ , we have, using Eqs.(1.25) and (1.27),

$$3P_1 = \mathcal{B}[\coth^2(t/\tau_U) - 4], \quad t \leq t_1, \tag{1.31}$$

while in the post-transition phase

$$3P_2 = \mathcal{B}\left(\frac{\tau_U}{t}\right)^2, \quad t \geq t_2. \tag{1.32}$$

Equating these two pressures with the critical pressure, Eq.(1.9), we obtain

$$\frac{3P_c}{\mathcal{B}} = \frac{3g_2}{\Delta g} = \coth^2\left(\frac{t_1}{\tau_U}\right) - 4 = \left(\frac{\tau_U}{t_2}\right)^2. \tag{1.33}$$

Equation (1.33) relates the time  $t_1$ , when the transition begins, to  $t_2$ , when it ends, and the fraction of degrees of freedom which are ‘freezing’ in the transition, in units of the  $\tau_U$ , Eq.(1.5).

We show the pressure and temperature in the Universe near hadronization in Fig. 1.3. The solid line corresponds to  $\alpha_s = 0.6$ , and  $\mathcal{B}^{1/4} = 195$  MeV, for which value  $\tau_U = 36 \mu\text{s}$ . Dotted lines are for  $\mathcal{B}^{1/4} = 170$  MeV and  $\mathcal{B}^{1/4} = 220$  MeV; a higher value of  $\mathcal{B}^{1/4}$  leads to a shorter time scale, Eq.(1.5).

It is straightforward to obtain the values of  $t_1$  and  $t_2$ . Using Eq.(1.14),  $g_2 = 19$ , and Eq.(1.15),  $\Delta g = 14$ , we find that the transition is complete at  $t_2 = 0.5\tau_U$ . The onset of the transition is found at  $t_1 = 0.37\tau_U$ , and the transition lasts  $0.13\tau_U$  in this case – the major uncertainty is related to the value of  $g_1 - g_2 = \Delta g$ . For the central value of  $\mathcal{B}^{1/4} = 195$  MeV with  $\tau_U = 36 \mu\text{s}$ , we find that the transition lasts  $\Delta t = (t_2 - t_1) = 4.7 \mu\text{s}$ .

The duration of the hadronization transition is comparable (35%) to the prior life span of the Universe in the deconfined phase. This time is exceedingly long compared with the time scale of hadronic interactions

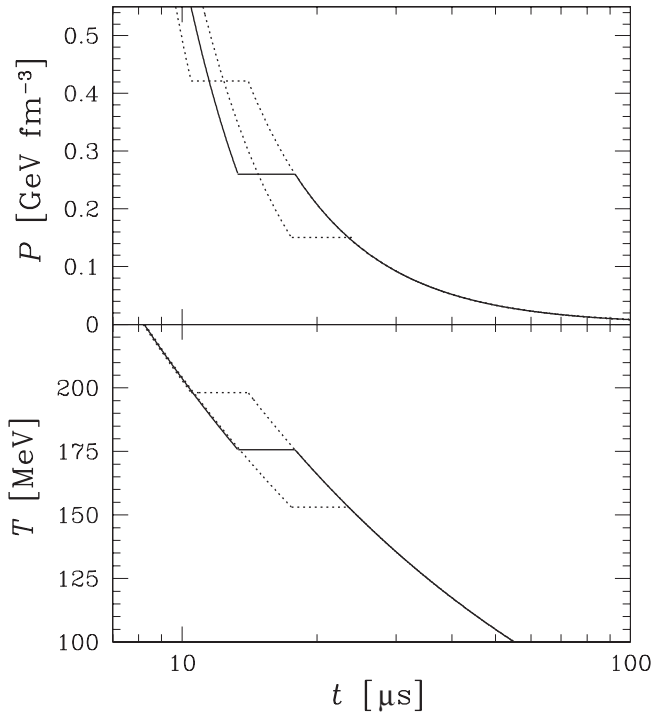


Fig. 1.3. Pressure (upper) and temperature (lower part) in the Universe, as function of time, in the vicinity of the phase transition from the deconfined phase to the confined phase. Solid lines,  $\mathcal{B}^{1/4} = 195$  MeV; dotted lines,  $\mathcal{B}^{1/4} = 170$  MeV (lower part) and  $\mathcal{B}^{1/4} = 220$  MeV (upper part) all for  $\alpha_s = 0.6$ .

( $10^{-22}$  s). It allows the decay of all unstable hadronic particles and, potentially, the development of domain structures. Moreover, the hadronization time is also three orders of magnitude longer than the characteristic time of hadronic weak decays, and is even longer than the decay time for a muon. What exactly happens to matter in this last phase transition in our Universe is not yet known. Studying dense matter in relativistic heavy-ion collisions should help us establish the physical laws governing this crucial epoch in the development of the Universe.

## 1.6 Looking for quark–gluon plasma: strangeness

How do we look for the phase transition of the primordial state of the Universe recreated for a short glimpse of time in the laboratory? How can we distinguish between the reactions involving confined hadronic particles only, and those in which we encounter the color-deconfined quarks and gluons?

- Is a transient new phase of matter, existing for a brief instant in time, perhaps for no more than  $10^{-22}$  s, in principle observable? This can be possible only if time-reversibility is broken more rapidly in the collision process. This will be the tacit assumption we make. How this occurs is one of the great open issues. In some sense on the time scale of  $10^{-23}$  s ‘measurement’ of the colliding system must be occurring, leading to the decoherence of the many-body quantum state.
- How can we observe a new phase of matter that exists for a short time, evolves and ultimately disintegrates (hadronizes) into usual final-state particles? At first sight, everything will always appear in the data very much akin to a reaction involving only the HG phase.

Considerable effort must be put into the understanding of the temporal and spatial evolution of the colliding system. We must identify the measurable quantities that can depend on the properties of the early and dense stage of collision, allowing us to penetrate the ‘nebula’ of the final hadronic state.

One observable is the quark chemical composition of the fireball of dense matter, which evolves as new quark flavors, such as strangeness, are cooked up inside the micro-bang fireball. Another observable is the entropy content: when quarks and gluons are liberated, the usually ‘frozen’ color bonds are broken and an entropy-rich state of matter is formed. We will address these two hadronic observables of QGP in greater detail in this book, and we offer here a first short overview of the related ideas and diagnostic methods.

The quarks ‘q’ (up ‘u’ and down ‘d’) from which the stable matter around us is made are easily produced as quark–antiquark pairs because they have small masses; see section 1.2. Another abundantly added quark flavor is strangeness, particularly if the deconfined QGP phase of matter is formed. Strangeness was one of the first proposed signatures of the deconfined phase [220]. The mass of strange quarks and antiquarks is of the same magnitude as the temperature  $T$  at which protons, neutrons, and other hadrons are expected to dissolve into quarks. This means that the abundance of strange quarks is sensitive to the conditions, structure, and dynamics of the deconfined-matter phase. The dominant mechanism for cooking up strangeness in quark–gluon deconfined matter was found to be the gluon-fusion reaction  $gg \rightarrow s\bar{s}$  [226]. We will address this process in depth in this book. Ultimately the quarks and antiquarks produced in the fireball of dense matter find their way into a multitude of final-state particles, with different quark contents, in the process of hadronization. This situation is illustrated in Fig. 1.4.

Detection of strange particles is facilitated by the fact that the massive strange quark decays into lighter quarks. Thus, strangeness-carrying

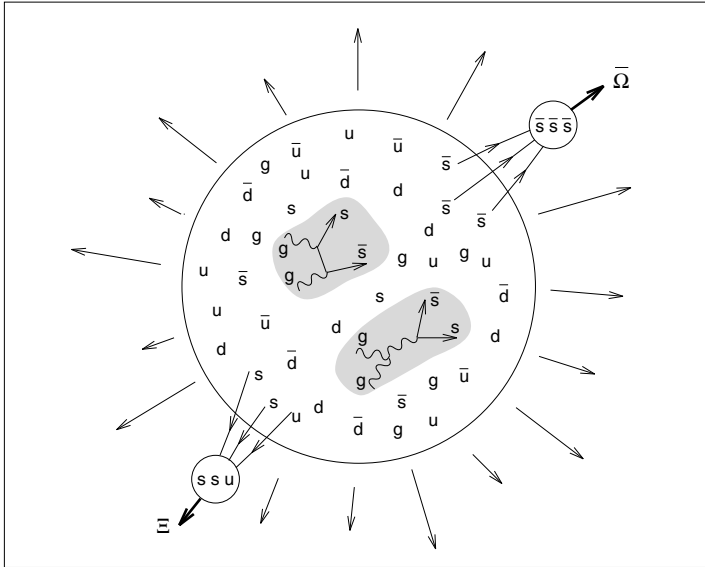


Fig. 1.4. A qualitative image of processes leading to production of (multi)-strange particles: in the QGP phase gluon collisions produce pairs of strange quarks, which are shown to assemble into otherwise rarely made multistrange baryons (for example  $\Xi(ssu)$ ) and antibaryons (for example  $\bar{\Omega}(\bar{s}\bar{s}\bar{s})$ ).

hadrons are naturally radioactive and decay by weak interactions that occur, in general, on a time scale that is extremely long compared with the nuclear-collision times. This makes it relatively easy to detect the strange particles through the tracks left by their decay products. It is important to remember that, unlike the light quarks, strange quarks are not brought into the reaction by the colliding nuclei. Therefore, we know for sure that any strange quarks or antiquarks observed in experiments have been made from the kinetic energy of colliding nuclei.

Should the new deconfined phase of matter be formed, we expect that final abundances of strange particles will be governed by (near) chemical equilibration of strangeness, i.e., that the yield abundance of QGP strangeness will saturate all available phase-space cells, making it into a  $q\bar{q}s\bar{s}g$  liquid. The total strangeness yielded is thus of considerable interest and is being measured as a function of the collision energy.

The excitation function of strangeness can be qualitatively studied by evaluating the ratio  $K^+(\bar{s}u)/\pi^+(\bar{d}u)$  shown in Fig. 1.5. Data obtained at several experimental facilities is shown: from the KaoS experiment at the SIS/GSI; from the E917 and E866 experiments at the AGS/BNL, from NA49 and NA44 experiments at the SPS/CERN, and from the STAR experiment at the RHIC/BNL. As long as the production of strange an-

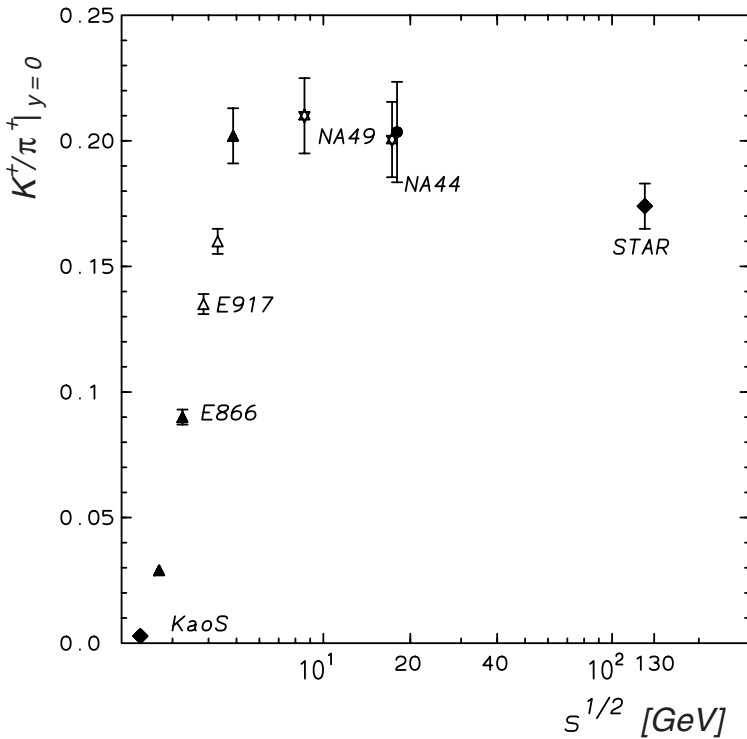


Fig. 1.5. Mid-rapidity  $K^+(\bar{s}u)/\pi^+(\bar{d}u)$  in reactions of the heaviest nuclei as a function of the collision energy. See the text for details.

tibaryons is small, the  $K^+(\bar{s}u)/\pi^+(\bar{d}u)$  ratio characterizes accurately the relative abundance of strangeness. This is not the case at RHIC energies, for which the strangeness content found in baryonic degrees of freedom is not negligible; see section 19.4. Using the estimate presented there, we find that

$$\frac{K^+ + \langle \bar{s} \rangle_Y}{\pi^+} \simeq 0.23,$$

where the second term  $\langle \bar{s} \rangle_Y$  is the strangeness content in the baryonic degrees of freedom.

This shows that the ratio of strangeness to hadron multiplicity continues to grow as the collision energy is increased. Since this growth is here seen to occur relative to the hadron multiplicity, measured in terms of the yield of positively charged pions, this implies that the yield of strangeness increases faster than the increase in production of entropy. At low energies the increase in yield of strangeness shown in Fig. 1.5 shows the effect of the energy threshold for production of strangeness.

The specific yield of strangeness per participating baryon increases much faster. In fact the specific yield of pions increases by 50% on going from AGS to CERN energies, which implies that the yield of strangeness per baryon continues to grow rapidly in the energy range  $5 \text{ GeV} < s^{1/2} < 17 \text{ GeV}$ .

The most interesting qualitative signature of strangeness in QGP is the yield of (multi)strange antibaryons. Given the ready supply of (strange) quarks and antiquarks, otherwise rarely produced (strange) particles will be emerging from a deconfined phase. In particular, the formation of antimatter particles comprising strangeness is of interest [215]. These particles can be more readily assembled in the high-density deconfined environment. In Fig. 1.4, we illustrate the sequence of events that leads to the formation of these particles: microscopic reactions, predominantly involving fusion of gluons, form pairs of strange quarks, of which clusters are formed and emitted.

Enhanced production of strange particles has been predicted to occur in a QGP for each strange particle species, and to increase with the strangeness content of the particle [164, 215]. Such enhancements in the number of strange particles produced per participating nucleon have now been observed in, e.g., lead–lead (Pb–Pb) collisions, compared with expectations arising from studies of proton–proton (p–p) and proton–beryllium (p–Be) collisions, as is shown in Fig. 1.6. The enhancement for a particular particle is defined as the number of that particle produced per participating nucleon in Pb–Pb collisions, divided by the number produced per participating nucleon seen in p–Be interactions [38].

In Fig. 1.6 the  $h^-$  symbol denotes the yield enhancement of negatively charged hadrons, mainly negative pions. This result implies an enhancement by a factor 1.3 for all non-strange hadrons. Such an enhancement is natural if QGP is formed on account of the breaking of the color bonds, and the associated enhancement in number of accessible degrees of freedom compared with reaction scenarios involving confined hadrons. Later in this book we will discuss in depth the issues related to enhanced production of entropy in the deconfined phase.

We further see, in Fig. 1.6, that the production of particles that contain one strange quark, such as the neutral kaon  $K^0$  and the  $\Lambda$ -particle, is enhanced by a factor of about three; the enhancement factor rises to about five for the doubly strange  $\Xi$ -particle (and its antiparticle, the anti- $\Xi$ ), and more than ten for the yield of  $(\Omega + \bar{\Omega})$  particles, which contain three strange or antistrange quarks. The particles in the right-hand panel of Fig. 1.6 have no quarks in common with the colliding nucleons.

When one is interpreting these results as significant indicators for the formation of the deconfined state, it is important to be able to argue that both matter and antimatter particles were produced by the same

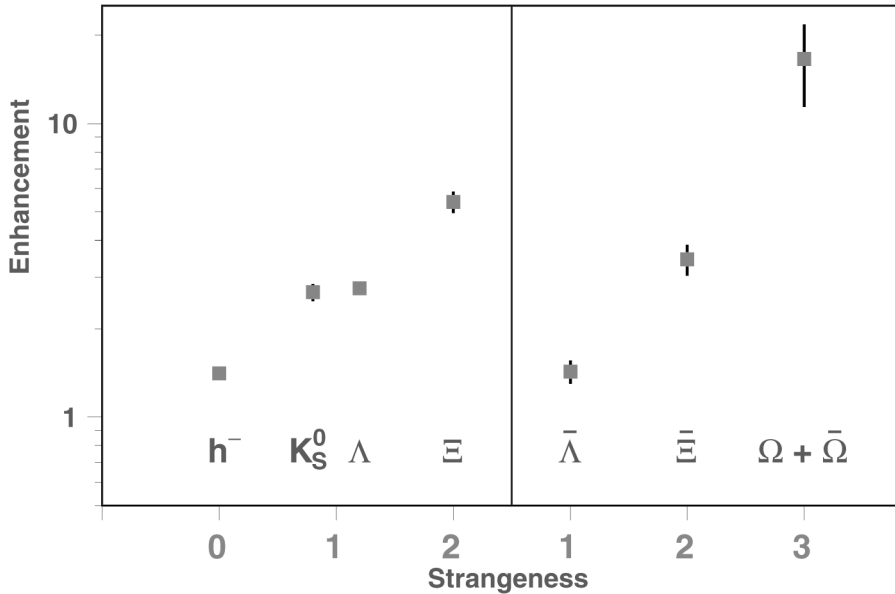


Fig. 1.6. Enhanced production of (strange) hadrons in Pb–Pb 158A-GeV heavy-ion collisions. Enhancement is defined with respect to p–Be collisions. Results were obtained by the CERN WA97 experiment considering particles emitted by a source stationary in the CM frame of reference [38].

mechanisms, as would be the case should a deconfined soup of quarks and antiquarks break up into final-state hadrons [42]. To demonstrate this, one studies not only the abundances but also the spectra of the particles produced. In order to reduce the dependence on the flow of matter along the collision axis, which is related to the collision dynamics, it is convenient to look only at hadron spectra with momentum components transverse to the original collision axis.

In Fig. 1.7, we see the spectra of strange baryons ( $\Lambda$ ,  $\Xi$ , and  $\Omega$ ) and antibaryons (anti- $\Lambda$ , anti- $\Xi^-$ , and anti- $\Omega^-$ ) as functions of the transverse energy,  $m_{\perp} = \sqrt{m^2 + p_{\perp}^2}$ . The most significant feature of Fig. 1.7 is that the slopes of the spectra for a particle and its antiparticle are very similar. The difference between the particle and antiparticle yields is a result of the quark–antiquark yield asymmetry present. The shape identity of matter and antimatter verifies that the mechanism of production is the same, corroborating the evidence for a common, deconfined source of strange hadrons.

Much of the material of this book will be devoted to the development of ideas demonstrating that these results are a natural consequence of the formation of the deconfined QGP state. It is important to keep in mind

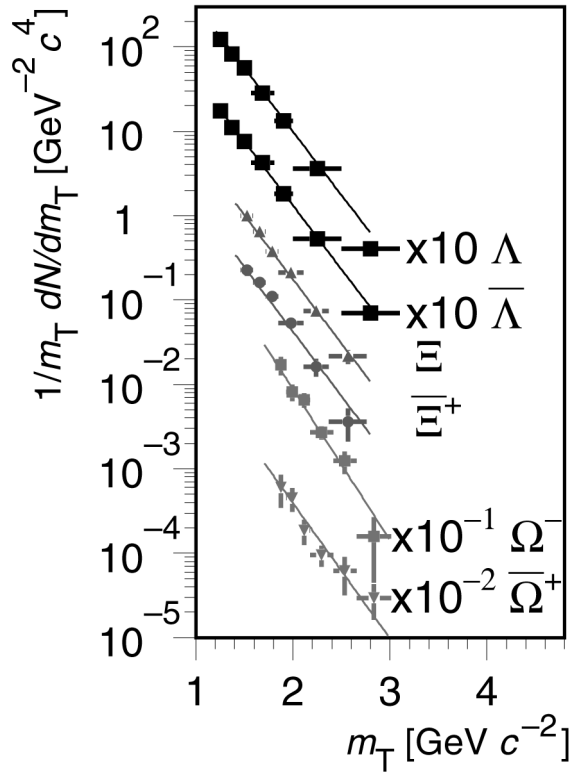


Fig. 1.7. Transverse mass spectra of strange and multistrange baryons and antibaryons. Results obtained by the CERN WA97 experiment for particles emitted at mid-rapidity [42].

that further evidence for the deconfinement of quarks in these reactions is available. The production of charmonium, i.e., particles containing a heavy charm quark and an antiquark, is another well-studied phenomenon [188].

### 1.7 Other probes of quark–gluon plasma

Since the charm quark is about ten times heavier than the strange quark, at SPS energies pairs of charm quarks can be formed only during the very early stages of the collision, as the nuclei begin to penetrate each other. In this early stage the colliding particles have the energy to overcome the higher energy threshold. If the QGP phase is formed, these charmed quarks have less chance of forming a charmonium state, because the gluons present within the plasma hinder their binding, or/and break the bound states. The observed strong suppression of the  $J/\Psi$  signal in 158A-GeV

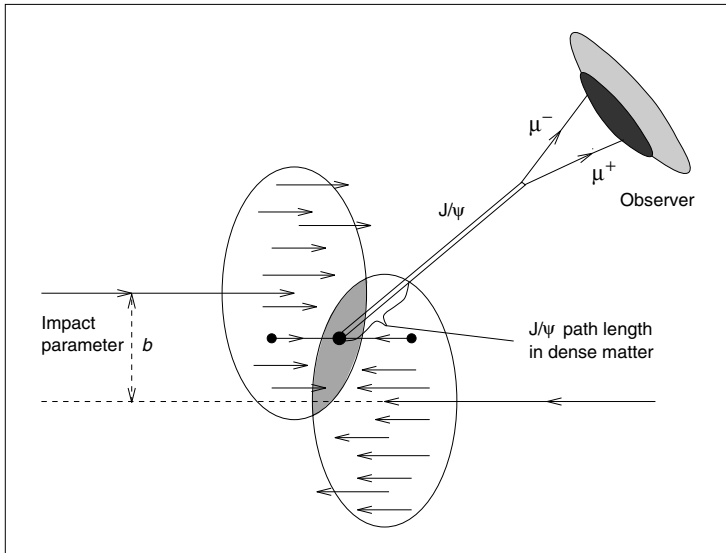


Fig. 1.8. The CM picture of initial moments of nuclear collision and an illustration of the path traveled by  $J/\Psi$  in dense matter.

Pb–Pb reactions is interpreted as being due to interactions with gluons. We will not develop this interesting topic in this book beyond a brief introduction, which follows.

Seen in the CM frame, the preformed  $J/\Psi$  must subsequently travel through a fireball of dense matter formed in the collision; see Fig. 1.8. The path in dense matter varies depending on the impact parameter, allowing one to evaluate the interaction (absorption) strength. This effect is particularly strong in most central collisions of nuclei.

The experimental  $J/\Psi$  yields, seen in Fig. 1.9, show clearly the unusual interaction strength of  $J/\Psi$ , when the path in dense matter is large as characterized by large values of the transverse energy generated by particle interactions. The  $J/\Psi$  is observed, in the NA50 experiment, by virtue of its decay into  $\mu^+\mu^-$  [12]. In Fig. 1.9, the yield of  $J/\Psi$  is obtained with reference to the yield of the dimuon background, which is believed to scale just like  $J/\Psi$  with the number of participant nuclei. We see, in Fig. 1.9 at  $E_\perp > 50$  GeV, a lesser increase in the suppression up to the last bins  $E_\perp > 120$  GeV. It is this rapid two-fold increase in the suppression as a function of  $E_\perp$  which makes an interpretation of these results, in terms of confined matter alone, difficult.

Considering quantitatively only the absorptive effect of the QGP, practically no  $J/\Psi$  should be observed for most central collisions at the higher energies available at the RHIC. However, representing the absorption of

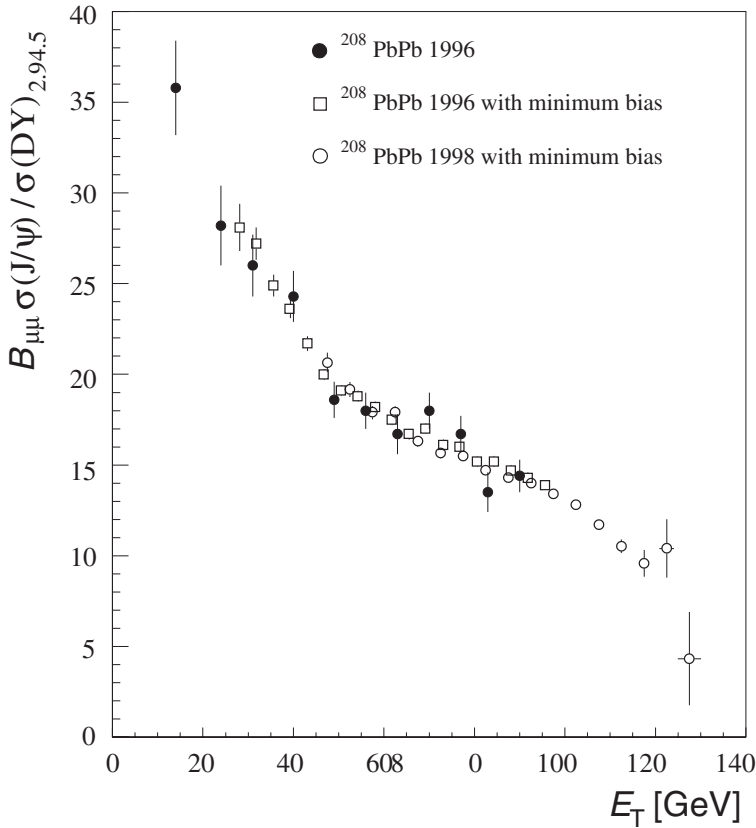
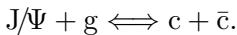


Fig. 1.9. Suppression of production of  $J/\Psi$  as a function of AA-collision centrality, characterized in terms of the transverse energy  $E_T$  produced in the reaction. Results of experiment NA50 [12].

the  $J/\Psi$  as a result of its interaction with the gluon content of QGP, one is led to consider the reverse reaction, and both break-up and formation become possible in the QGP medium:



Depending on the absolute abundance of open charm, there could be considerable in-plasma production of  $J/\Psi$ . A quantitative study of this effect has recently been carried out [257], resulting in the prediction of an enhancement in production of  $J/\Psi$  in central nuclear collisions in the energy range accessible at the RHIC. Observation of this new mechanism of  $J/\Psi$  formation would constitute proof of the mobility of charmed quarks in the fireball of dense matter.

If this changing pattern of  $J/\Psi$  suppression turning into enhancement is confirmed experimentally to be present relative to the directly measured yield of ‘open’ charm, with the expected energy dependence and centrality dependence (peripheral interactions agree with extrapolations from p-induced reactions), this will constitute convincing evidence for the formation of the deconfined form of matter.

Charmed hadrons, i.e., particles with ‘open’ charm, have not yet been observed directly, but considerable effort is being made today to prepare experiments at the SPS, RHIC and LHC that will have the capability to detect them. The experimental difficulty is the rapid disintegration of charmed hadrons, requiring an extremely precise tracking of particles beginning very near to the interaction vertex. The availability of direct measurements of the abundance of charm would provide a reliable baseline for understanding the phenomenon of suppression of production of  $J/\Psi$ , and perhaps at higher energies than those at the SPS, enhancement of its production.

A few further signatures of deconfinement have also been proposed. Akin to the disappearance of  $J/\Psi$ , jets of hadrons produced by hard quarks and gluon arising from initial interactions should disappear due to the enhanced strength of interaction in the ‘colored’ charge plasma of the deconfined medium [72]. There is very little doubt that this idea works. However, this rapid quenching of hard particles is the mechanism of thermalization of partons, aside of being a direct signature for a new phase of matter. This mechanism provides the motivation for the statistical description of the properties of dense matter. Can the thermalization of partons be seen as a signature of QGP? We will not address in this book this rapidly developing subject.

Photons  $\gamma$  and lepton pairs emerging from the decay of virtual photons  $\gamma^* \rightarrow e^+e^-$  and  $\mu^+\mu^-$  are, at first sight, the most promising probes of the dense hadronic matter [120, 154, 244]. Electromagnetic interactions are strong enough to lead to an initial detectable signal, with secondary interactions being too weak to alter substantially the shape and yield of the primary spectra. Direct photons and leptons contain information about the properties of dense matter in the initial moments of the collision. Of particular interest would be the possible exploration of the initial time period leading to the formation of thermal equilibrium.

Therefore, at first, photons and lepton pairs (often also called dileptons) originating from QGP, produced, e.g., by quark–antiquark annihilation, were considered to be the primary diagnostic tool, just as photons are a powerful diagnostic for traditional (electromagnetic) plasmas. However, thousands of particles are created in high-energy nuclear collisions. Among those the decay of neutral  $\pi^0$  mesons is known to produce a strong

background. It is very difficult to extract the direct QGP photon signal, which is only a small fraction of all photons produced.

Because dilepton formation, compared with formation of photons, requires one additional electromagnetic interaction, the yield of dileptons is considerably smaller, by a factor 300 or more, than the yield of direct photons. However, the dilepton background is also much reduced. While the directly produced photons are present at the level of 5% of the photon signal observed, the amount of dileptons from formation of dense matter is believed to exceed the background by a factor as large as 3–5. However, dileptons have been shown to have other origins related to properties of confined hadronic matter and the observed pattern of dilepton production, given the large systematic experimental error, is difficult to interpret [22]. We will not dwell on this complex subject in this book.

The diagnostic strength of the strangeness signature, in comparison with direct photons and dileptons, is that, aside from the overall enhancement of abundance, we also have the pattern of enhancement shown in Fig. 1.6, and the matter–antimatter symmetry seen in Fig. 1.7. The yield of strangeness is related to the initial most extreme conditions of the QGP phase, much like the photon and dilepton yields. However, strangeness has relatively little background. The source of strangeness, gluons, is by far more characteristic for the new phase of matter than is the source of photons and dileptons, which are electrical currents of quarks, present both in the confined and in the deconfined state of matter.

## 2 Hadrons

### 2.1 Baryons and mesons

As the above first and qualitative discussion of signals of QGP formation has shown, to pursue the subject we next need to understand rather well the properties of ‘elementary’ particles, and specifically strongly interacting (hadronic) particles. These are complex composites of the more elementary strongly interacting particles: quarks and gluons. Quark-composite hadronic particles are final products emerging from heavy-ion collisions, and play an important role in this book – there are two different types of colorless quark bound states: baryons, comprising three valence quarks, and mesons, which are quark–antiquark bound states.

Typically, each type of (composite) hadron has many resonances, i.e., states of greater mass but the same quantum number, which are generally internal structural excitations of the lowest-mass state. Normally the lowest-mass states of a given quantum number are stable (that is, if they decay, it occurs very slowly compared with the time scale of hadronic reactions), but there are notable exceptions, such as the  $\Delta$ -resonances,